

**In-orbit calibration strategy for ocean color sensors**

by

Howard R. Gordon

Department of Physics

University of Miami

Coral Gables, FL 33124

Submitted to *Remote Sensing of Environment*

The author is grateful for support from the National Aeronautics and Space Administration under Grant NAGW-273 Contracts NAS5-31363 and NAS5-31734.

## Abstract

To recover the ocean water-leaving radiance and derive biophysical parameters from observations of space-borne ocean color sensors, the required uncertainty in the measured top-of-atmosphere radiance is at present impossible to achieve prior to launch. A methodology and strategy for achieving the required uncertainty in the post-launch era is presented here. The method consists of combining direct measurements of the water-leaving radiance, whitecap radiance, and aerosol optical thickness made simultaneously with satellite overpasses, with radiative transfer theory to reduce the calibration uncertainty of the visible bands with respect to the near-infrared (NIR). This procedure is possible over the open ocean where, in the absence of aerosol transported from land over long distances by the wind, the atmosphere can be very clear with most of the aerosol generated by local processes such as breaking waves, e.g., the aerosol optical thickness in the visible  $\sim 0.05$ – $0.10$ . In this case, the radiative transfer process is considerably simplified and molecular scattering is the dominant atmospheric component in the visible. It is shown that such a procedure alone is sufficient to reduce the calibration uncertainty to required levels. Further reduction is possible by reducing the uncertainty in the NIR calibration by measuring sky radiance from island locations (or a ship), and using these to predict the at-sensor radiance. For the most part, this NIR calibration is limited by the uncertainty in the calibration of the radiometer used to measure the sky radiance. Finally, the sensor calibration is maintained by monitoring the actual water-leaving radiance continuously at a single location, where the atmosphere is sufficiently clear that atmospheric correction introduces only a small error, and directly comparing the true and the sensor-derived water-leaving radiances.

## 1. Introduction

Several ocean color sensors are expected to be launched within the next few years, e.g., SeaWiFS [Hooker *et al.*, 1992] and MODIS [Salomonson *et al.*, 1989], for the purpose of understanding oceanic primary production on a global scale. As the information-containing radiance backscattered out of the water and transmitted to the top of the atmosphere (TOA) is only a small portion of the radiance that they measure, these sensors require an accuracy in radiometry that cannot be achieved pre-launch. There are several issues concerning radiometric calibration that must be addressed for each ocean color sensor. For example, when there are bright clouds in a scene, how close to the clouds will the radiometry be valid, i.e., not corrupted by the presence of the clouds? If sensors employ array detectors (MODIS), do all of the individual detectors in a given spectral band in the array record the same radiance when viewing a uniform scene? Most issues such as these can be resolved through a systematic examination of the imagery, or through small radiometric calibration adjustments of one detector relative to another in an array. However, in the latter case, even if all detectors provide the same values for the radiance when viewing a uniform scene, what is the uncertainty in that value? In this paper, we provide the methodology and the measurement requirements for reducing this latter uncertainty to acceptable levels in the post-launch era.

The radiance reflected from the ocean itself consists of two components (1) the radiance reflected from the sea surface (diffuse reflection from whitecaps and direct Fresnel-reflection from the interface), and (2) radiance backscattered *out* of the water from beneath the surface. The latter is referred to as the water-leaving radiance,  $L_w$ . It contains the desired information [Gordon and Morel, 1983]. In what follows, we will replace radiance  $L$  by reflectance  $\rho$  defined through  $\rho = \pi L / F_0 \cos \theta_0$ , where  $\theta_0$  is the solar zenith angle, and  $F_0$  is the extraterrestrial solar irradiance. At a given wavelength,  $\lambda$ , the water-leaving reflectance is related to the reflectance observed at the sensor ( $\rho_t$ ) through

$$\rho_t(\lambda) = \rho_r(\lambda) + \rho_a(\lambda) + \rho_{ra}(\lambda) + t(\lambda)\rho_w(\lambda) + t(\lambda)\rho_{wc}(\lambda) + T(\lambda)\rho_g(\lambda), \quad (1)$$

where  $\rho_r(\lambda)$  is the contribution from pure Rayleigh (molecular) scattering,  $\rho_a(\lambda)$  the contribution from pure aerosol scattering,  $\rho_{ra}(\lambda)$  the contribution due to the interaction effect between air molecules and aerosols,  $t(\lambda)\rho_{wc}(\lambda)$  the contribution from whitecaps,  $T(\lambda)\rho_g(\lambda)$  the contribution from direct sun glitter, and  $t(\lambda)\rho_w(\lambda)$  the desired water-leaving reflectance propagated to the TOA.  $T$  is the direct transmittance and  $t$  is the diffuse transmittance of the atmosphere. In Eq. (1),  $\rho_r$ ,

$\rho_a$ , and  $\rho_{ra}$  are understood to include the interactions with the sea surface, e.g.,  $\rho_r$  is the reflectance of a Rayleigh-scattering atmosphere bounded by a Fresnel-reflecting ocean that absorbs all photons penetrating through its interface. Typically, in clear water, the contribution of  $t\rho_w$  to  $\rho_t$  is  $\sim 10\%$  in the blue ( $\lambda \sim 440$  nm), 5% in the green ( $\lambda \sim 550$  nm) and negligible in the near infrared (NIR,  $\lambda \gtrsim 750$  nm).

In Eq. (1)  $\rho_r$  can be precisely computed given the surface atmospheric pressure [Gordon, Brown and Evans, 1988], and  $\rho_{wc}$  can be estimated given the wind speed [Frouin, Schwindling and Deschamps, 1996; Gordon and Wang, 1994a; Moore, Voss and Gordon, 1997]. As  $\rho_g$  is very large near the specular image of the sun, it is required that viewing directions be chosen such that it is negligible. The terms involving aerosols,  $\rho_a + \rho_{ra}$ , are highly variable, and in the blue are comparable in magnitude to  $t\rho_w$  [Gordon, 1997]. Thus, the principal difficulty in retrieving  $t\rho_w$  from  $\rho_t$  is assessing the aerosol contribution.

Gordon and Wang [1994b] have developed an algorithm for retrieving  $t\rho_w$  from  $\rho_t$  assuming that  $\rho_r$  is computed from an estimate of the surface pressure,  $\rho_{wc}$  has been determined from an estimate of the wind speed, and  $\rho_g$  is negligible. This algorithm has been shown to be capable of retrieving  $t\rho_w$  at 443 nm with an uncertainty  $\lesssim \pm 0.002$ , when the aerosol over the ocean is nonabsorbing or only weakly absorbing [Gordon, 1997]. This uncertainty meets the goal of both SeaWiFS and MODIS: a 5% uncertainty in the water leaving reflectance in the blue in very clear ocean water [Hooker et al., 1992]. In the Gordon and Wang algorithm, the aerosol contribution and its spectral variation are assessed utilizing bands in the NIR, where  $\rho_w$  can be assumed to be  $\sim 0$  due to the strong absorption of liquid water there. Aerosol models are used to extrapolate the aerosol contribution from the NIR to the visible, and also to account for the effects of multiple scattering.

## 2. Effect of calibration errors

Since the desired water-leaving reflectance is only a small part of  $\rho_t$ , accurate calibration of the sensor is critical [Gordon, 1987]. For example, if  $t\rho_w$  is 10% of  $\rho_t$ , and we want  $\rho_w$  with an uncertainty of  $\pm 5\%$ , one would expect that it would be necessary to know  $\rho_t$  with an uncertainty of no more than  $\pm 0.5\%$ . However, as several bands are used in the atmospheric correction of a single

band, the variation of the calibration error from band to band is also important. We now describe simulations to estimate the magnitude of the effect of the radiometric calibration error.

To assess the effect of calibration errors,  $\rho_t$  pseudo data were simulated using the *Shettle and Fenn* [1979] maritime aerosol model with 80% relative humidity (M80). In the absence of calibration errors, the performance of the Gordon and Wang algorithm is excellent for this aerosol model. An error was then added to each of the pseudo measured reflectances, i.e.,

$$\rho'_t(\lambda) = \rho_t(\lambda)[1 + \alpha(\lambda)], \quad (2)$$

where  $\alpha(\lambda)$  is the fractional error in  $\rho_t(\lambda)$ , and  $\rho'_t(\lambda)$  is the value of  $\rho_t(\lambda)$  that the incorrect sensor calibration would indicate. The Gordon and Wang correction algorithm was then operated using the incorrect  $\rho'_t(\lambda)$  as the measured value, rather than the correct  $\rho_t(\lambda)$ , and the error in the retrieved  $t\rho_w(\lambda)$ , was computed.

The resulting error at 443 nm is presented in Figures 1a–1d, for a sensor viewing near the edge of the scan (viewing nadir angle  $\sim 45^\circ$ ) in the perpendicular plane, as a function of  $\theta_0$ . The  $y$ -axis in these figures is the error in the retrieved  $t\rho_w$ , indicated by  $\Delta\rho(\theta_0)$ . Figures 1a and 1b are for  $\alpha(765) = \alpha(865)$  with  $\alpha(443) = 0$  (Figure 1a) and  $\alpha(443) = \alpha(765) = \alpha(865)$  (Figure 1b). These show the effect of a calibration error that has the same magnitude and sign at both 765 and 865 nm. In contrast, Figures 1c and 1d show the effect of having calibration errors that have a much smaller magnitude but opposite signs at 765 and 865 nm. In this case even a small calibration error (1%) can have an effect similar to a large calibration error (5%) when the signs are all the same. As we shall see later, the reason the error is so much larger when it is of opposite sign at 765 and 865 nm is that it will cause an error in the estimated spectral variation of the aerosol component that will propagate through the atmospheric correction algorithm.

The goal for the pre-launch calibration of the relevant ocean color bands on SeaWiFS and MODIS is that  $L_t$  have an uncertainty of  $< \pm 10\%$  and  $5\%$ , respectively. Figure 1 demonstrates that such an error would cause the error in the retrieved  $\rho_w(443)$  to be far outside the acceptable range ( $\pm 0.002$ ). A method for overcoming these calibration difficulties is provided below.

### 3. Radiative transfer in the aerosol single-scattering approximation

Over the open ocean the atmosphere can be very clear with most of the aerosol generated by local processes such as breaking waves. Such an aerosol is almost nonabsorbing and the aerosol optical thickness at 550 nm is often in the range 0.05–0.10 [Korotaev *et al.*, 1993; Reddy *et al.*, 1990; Villevalde *et al.*, 1994]. Under such conditions, a simple atmospheric correction algorithm that employs a multiply-scattered Rayleigh component and a singly-scattered aerosol component can be used to retrieve  $\rho_w$  [Gordon, 1997]. In this section we review the relevant radiative transfer for such an approximation.

When the aerosol concentration is small, it is possible to approximate the path reflectance  $\rho_r + \rho_a + \rho_{ra}$  by  $\rho_r + \rho_{as}$ , where  $\rho_r$  is the multiple-scattering reflectance of a pure Rayleigh-scattering atmosphere bounded by a totally-absorbing Fresnel-reflecting interface, and  $\rho_{as}$  is the aerosol contribution computed to first order in the aerosol optical thickness  $\tau_a$ . The aerosol contribution in this approximation is given by

$$\begin{aligned} \rho_{as}(\lambda) &= \omega_a(\lambda)\tau_a(\lambda)p_a(\theta_v, \phi_v; \theta_0, \phi_0; \lambda)/4 \cos \theta_v \cos \theta_0, \\ p_a(\theta_v, \phi_v; \theta_0, \phi_0; \lambda) &= P_a(\Theta_-, \lambda) + \left( r(\theta_v) + r(\theta_0) \right) P_a(\Theta_+, \lambda), \\ \cos \Theta_{\pm} &= \pm \cos \theta_0 \cos \theta_v - \sin \theta_0 \sin \theta_v \cos(\phi_v - \phi_0), \end{aligned} \quad (3)$$

where  $P_a(\Theta, \lambda)$  is the aerosol scattering phase function for a scattering angle  $\Theta$ ,  $\omega_a$  is the aerosol single scattering albedo, and  $r(\alpha)$  is the Fresnel reflectance of the interface for an incident angle  $\alpha$ . The angles  $\theta_0$  and  $\phi_0$  are, respectively, the zenith and azimuth angles of a vector from the point on the sea surface under examination (pixel) to the sun, and likewise,  $\theta_v$  and  $\phi_v$  are the zenith and azimuth angles of a vector from the pixel to the sensor. The zenith angles are measured with respect to the *upward* normal.

Thus, in the single-scattered aerosol approximation to the radiative transfer in the atmosphere, and ignoring whitecaps and sun glitter, we have

$$\rho_t(\lambda) = \rho_r(\lambda) + \rho_{as}(\lambda) + t(\lambda)\rho_w(\lambda). \quad (4)$$

Using this equation it is easy to devise an atmospheric correction algorithm [Wang and Gordon, 1994]. Consider two spectral bands in the near infrared (NIR) at  $\lambda_s$  and  $\lambda_l$ , where the subscript “s” stands for short and “l” for long. These bands are assumed to possess the attribute that  $\rho_w \approx 0$ ,

because of the strong absorption by liquid water in the NIR. For MODIS  $\lambda_s = 750$  nm and  $\lambda_l = 865$  nm, while for SeaWiFS  $\lambda_s = 765$  and  $\lambda_l = 865$ . Then Eq. (4) provides  $\rho_r + \rho_{as}$  at both  $\lambda_s$  and  $\lambda_l$ . The quantity  $\rho_r(\lambda)$  can be computed accurately, so  $\rho_{as}(\lambda_s)$  and  $\rho_{as}(\lambda_l)$  can be determined from the values of  $\rho_t - \rho_r$  at  $\lambda_s$  and  $\lambda_l$ , allowing estimation of the parameter  $\varepsilon(\lambda_s, \lambda_l)$ :

$$\varepsilon(\lambda_s, \lambda_l) \equiv \frac{\rho_{as}(\lambda_s)}{\rho_{as}(\lambda_l)} = \frac{\omega_a(\lambda_s)\tau_a(\lambda_s)p_a(\theta_v, \phi_v; \theta_0, \phi_0; \lambda_s)}{\omega_a(\lambda_l)\tau_a(\lambda_l)p_a(\theta_v, \phi_v; \theta_0, \phi_0; \lambda_l)}. \quad (5)$$

If we can find a way to compute the value of  $\varepsilon(\lambda_i, \lambda_l)$  for the band at  $\lambda_i < \lambda_s$  from the measured value of  $\varepsilon(\lambda_s, \lambda_l)$ , we can compute  $\rho_{as}(\lambda_i)$ , which, when combined with  $\rho_t(\lambda_i)$  and  $\rho_r(\lambda_i)$ , provides  $\rho_w(\lambda_i)$ :

$$t(\lambda_i)\rho_w(\lambda_i) = \rho_t(\lambda_i) - \rho_r(\lambda_i) - \varepsilon(\lambda_i, \lambda_l)\rho_{as}(\lambda_i). \quad (6)$$

The key to utilizing this procedure is to be able to estimate  $\varepsilon(\lambda_i, \lambda_l)$  from the measured  $\varepsilon(\lambda_s, \lambda_l)$ . Using a set of aerosol models developed by *Shettle and Fenn* [1979], *Wang and Gordon* [1994] showed that to a good approximation

$$\varepsilon(\lambda_i, \lambda_l) = \exp[c(\lambda_l - \lambda_i)]. \quad (7)$$

Further examples of the validity of this approximation are provided in *Gordon* [1997]. Using this it is easy to complete the retrieval of  $t(\lambda_i)\rho_w(\lambda_i)$ :

$$t(\lambda_i)\rho_w(\lambda_i) = \rho_t(\lambda_i) - \rho_r(\lambda_i) - \varepsilon^{(e)}(\lambda_i, \lambda_l)\rho_{as}(\lambda_i). \quad (8)$$

In Eq. (8),  $\varepsilon^{(e)}(\lambda_i, \lambda_l)$  is the estimated value of  $\varepsilon(\lambda_i, \lambda_l)$  assuming the exponential variation with  $\lambda_i$ , i.e.,

$$\varepsilon^{(e)}(\lambda_i, \lambda_l) \equiv \exp[c(\lambda_l - \lambda_i)] = \exp \left[ \left( \frac{\lambda_l - \lambda_i}{\lambda_l - \lambda_s} \right) \log_e \left( \frac{\rho_{as}(\lambda_s)}{\rho_{as}(\lambda_l)} \right) \right].$$

*Gordon* [1997] shows that excellent results can be obtained with this simple algorithm when the aerosol is nonabsorbing or weakly absorbing, and the aerosol optical thickness at  $\lambda_l$  (865 nm) is  $\lesssim 0.10$ . In the case of SeaWiFS, correction for the effect of the O<sub>2</sub> “A” absorption band are necessary at  $\lambda_s$  [*Ding and Gordon*, 1995].

We now use this aerosol single-scattering approximation to understand analytically the effects of the calibration errors that are shown in Figure 1. Assuming the aerosol single-scattering formulation of the radiative transfer process is exact, and using Eq. (7), to first order in  $\alpha(\lambda)$  the error in the retrieved  $\rho_w$  is [*Gordon*, 1997]

$$t(\lambda_i)\Delta\rho_w(\lambda_i) = \alpha(\lambda_i)\rho_t(\lambda_i) - \varepsilon(\lambda_i, \lambda_l)\alpha(\lambda_l)\rho_t(\lambda_l) - \left( \frac{\lambda_l - \lambda_i}{\lambda_l - \lambda_s} \right) \left[ \frac{\varepsilon(\lambda_i, \lambda_l)}{\varepsilon(\lambda_s, \lambda_l)} \alpha(\lambda_s)\rho_t(\lambda_s) - \varepsilon(\lambda_i, \lambda_l)\alpha(\lambda_l)\rho_t(\lambda_l) \right]. \quad (9)$$

In Eq. (9), the first term,  $\alpha(\lambda_i)\rho_i(\lambda_i)$ , represents the direct effect of any calibration error at  $\lambda_i$  on the retrieved  $\rho_w(\lambda_i)$ . The remaining terms represent the indirect effect resulting from calibration error at  $\lambda_s$  and  $\lambda_l$ . Note that if  $\lambda_s$  and  $\lambda_l$  have calibration errors with the same sign, the second term will subtract from the first, and cancelation in the terms in the square brackets will also occur. In contrast, if  $\alpha(\lambda_s)$  and  $\alpha(\lambda_l)$  have different signs, the error is magnified as the two terms in the square brackets in Eq. (9) will add. This explains the behavior of the error in  $t\rho_w$  in Figures 1c and 1d.

#### 4. Calibration initialization

In Section 2 examples were provided to show the sensitivity of the algorithm to sensor calibration errors (Figure 1). It was demonstrated that calibration errors of the order of  $\pm 5\%$ , the absolute radiometric calibration uncertainty specified for the MODIS visible bands, would lead to excessive error in  $\rho_w$ , even if the calibration error in the two NIR bands were of the same sign. When errors in these bands are small ( $\sim \pm 1\%$ ) but have opposite signs (Figures 1c and 1d), the error in the water-leaving reflectance becomes large because of the extrapolation of  $\epsilon$  into the visible [Eq. (9)]. Thus, it is clear that the calibration uncertainty of SeaWiFS and MODIS must be reduced in order to provide acceptable  $\rho_w$  retrievals.

Although the calibration requirement is difficult if not impossible to meet using standard laboratory methods, we show here that it should be possible to perform an adequate calibration in orbit using surface measurements to deduce the true water-leaving radiance and the optical properties of the aerosol. This is normally referred to as *vicarious* calibration [Evans and Gordon, 1994; Fraser and Kaufman, 1986; Gordon, 1987; Koepke, 1982; Slater et al., 1987]. We now outline a methodology for effecting such calibration, the process of which we refer to as *initialization*. This calibration is *not* radiometric, rather, it is a calibration of the entire system — the sensor *plus* the algorithms. As will be seen below, the sensor calibration will be adjusted to force the algorithm to conform to surface measurements of water-leaving radiance and atmospheric (aerosol) properties. A similar procedure was carried out for CZCS [Evans and Gordon, 1994], but without surface-based atmospheric measurements. It was only moderately successful because the calibration of that instrument varied in time, and there was no independent way of determining the temporal variation. Here, we make the assumption that any change in the sensitivity of the instrument with

time can be determined by other methods, e.g., using an on-board solar diffuser or imaging the moon.

Upon initial operation of the sensor, one expects that the  $\alpha(\lambda_i)$  in Eq. (2) will be of the order of  $\pm 5\%$  (MODIS), with  $\alpha(\lambda_i)$  being positive for some of the  $\lambda_i$ 's and negative for others. We acquire imagery over ships measuring  $L_w(\lambda_i)$  for a variety of (clear sky) aerosol concentrations. Given  $\rho_w(\lambda_i)$ , and assuming the atmospheric correction algorithm [Eq. (6)] is exact, we operate it backward, i.e., compute  $\varepsilon(\lambda_i, \lambda_l)$  using  $\rho_w(\lambda_i)$  at each wavelength  $\lambda_i$ . This provides the behavior of  $\varepsilon(\lambda_i, \lambda_l)$  with  $\lambda_i$ . It is expected to be a smooth, nearly exponential [Gordon, 1997; Wang and Gordon, 1994], function of  $\lambda_i$ . If the  $\alpha(\lambda_i)$ 's differ significantly in magnitude (or in sign),  $\varepsilon(\lambda_i, \lambda_l)$  will vary with  $\lambda_i$  in a repeatable (from day-to-day) but unrealistic manner, and this will be magnified when the aerosol optical thickness is small.

To understand this magnification, we assume that the aerosol single-scattering version of the radiative transfer is exact. In that case,

$$\rho_t(\lambda) = \rho_r(\lambda) + \rho_{as}(\lambda) + t(\lambda)\rho_w(\lambda),$$

and from its definition

$$\varepsilon(\lambda_i, \lambda_l) = \frac{\rho_{as}(\lambda_i)}{\rho_{as}(\lambda_l)} = \frac{\rho_t(\lambda_i) - \rho_r(\lambda_i) - t(\lambda_i)\rho_w(\lambda_i)}{\rho_t(\lambda_l) - \rho_r(\lambda_l) - t(\lambda_l)\rho_w(\lambda_l)}.$$

Inserting  $\rho_t'$  from Eq. (2) in place of  $\rho_t$ , we have the apparent value of  $\varepsilon(\lambda_i, \lambda_l)$ :

$$\varepsilon'(\lambda_i, \lambda_l) = \frac{\alpha(\lambda_i)\rho_t(\lambda_i) + \rho_{as}(\lambda_i)}{\alpha(\lambda_l)\rho_t(\lambda_l) + \rho_{as}(\lambda_l)}. \quad (10)$$

For very small  $\alpha(\lambda)$ 's this provides an approximately correct  $\varepsilon(\lambda_i, \lambda_l)$ , i.e.,  $\rho_{as}(\lambda_i)/\rho_{as}(\lambda_l)$ ; however, if the  $\alpha(\lambda_i)$ 's are not small, very significant errors in the computed  $\varepsilon(\lambda_i, \lambda_l)$  are possible. This error will be particularly large for bands for which  $\rho_t \gg \rho_{as}$ , e.g., in the blue. To illustrate this, a numerical example is useful. Consider two error scenarios: (1) the  $\alpha(\lambda_i)$ 's alternate in sign from band to band; and (2) the  $\alpha(\lambda_i)$ 's all have the same sign. In each case we assume for simplicity that the  $\alpha(\lambda_i)$  all have the same magnitude, and employ a viewing geometry specified by  $\theta_0 \approx 32^\circ$ ,  $\theta_v \approx 33^\circ$ , and  $\phi_v \approx 100^\circ$ . We take the "aerosol radiance"  $L_a$  defined as  $L_t - L_r - tL_w$  at 670 nm to be 0.2, 0.4, and 0.6 mW/cm<sup>2</sup>μm sr. These values correspond to  $\rho_{as} \approx 0.005, 0.010,$  and 0.015, or  $\tau_a \approx 0.04, 0.08,$  and 0.12 at 670 nm, respectively. For reference, from CZCS imagery, the mean  $L_a$  for the Arabian Sea in winter (the low aerosol season) is  $\sim 0.6$  mW/cm<sup>2</sup>μm sr, with a

standard deviation of about  $0.2 \text{ mW/cm}^2 \mu\text{m sr}$  (C.R. McClain, GSFC, personal communication). Thus,  $L_a$  values in this range are easily found over the oceans. The results of computing  $\varepsilon'(\lambda_i, \lambda_l)$  with Eq. (10) as a function of the magnitude and the sign of the calibration error are provided in Figures 2a–2d. In preparing the figures it has been assumed that the correct value of  $\varepsilon(\lambda_i, \lambda_l)$  is unity for all  $\lambda_i$ , i.e., what would be expected for a maritime aerosol at high relative humidity [Shettle and Fenn, 1979; Wang and Gordon, 1994]. The figures clearly show that the apparent value of  $\varepsilon(\lambda_i, \lambda_l)$  is strongly influenced by the calibration error, and that the influence increases as the aerosol optical thickness decreases. If the true value of  $\varepsilon(\lambda_i, \lambda_l)$  were known, the calibration for the band at  $\lambda_i$  could be adjusted to bring the apparent value into equality with the true value. That is, replacing  $\varepsilon'$  by the known  $\varepsilon$  in Eq. (10) shows that the residual value of  $\alpha(\lambda_i)$  is related to  $\alpha(\lambda_l)$  by

$$\alpha(\lambda_i) = \frac{\rho_t(\lambda_l)}{\rho_t(\lambda_i)} \varepsilon(\lambda_i, \lambda_l) \alpha(\lambda_l). \quad (11)$$

Thus, with this calibration adjustment, the residual error  $\alpha(\lambda_i)$  will be  $< \alpha(\lambda_l)$ , since  $\rho_t(\lambda_l) < \rho_t(\lambda_i)$  because of the strong spectral variation of  $\rho_r$ . We see that this form of calibration adjustment automatically reduces the error in the short-wave bands to a value below  $\alpha(\lambda_l)$  and assures that all of the  $\alpha$ 's have the same sign as  $\alpha(\lambda_l)$ .

In practice Eq. (11) is useless because  $\alpha(\lambda_l)$  is unknown. Thus, given  $\varepsilon(\lambda_i, \lambda_l)$  one must actually adjust the calibration by trial and error until  $\varepsilon'(\lambda_i, \lambda_l)$  agrees with the correct value. This is equivalent to (1) solving Eq. (8) for  $\rho_t(\lambda_i)$ , given  $t(\lambda_i)\rho_w(\lambda_i)$  and replacing  $\varepsilon^{(e)}(\lambda_i, \lambda_l)$  by  $\varepsilon(\lambda_i, \lambda_l)$ , and (2) adjusting the sensor calibration to force  $\rho_t'(\lambda_i)$  into agreement with the computed  $\rho_t(\lambda_i)$ . This was done for the example in Figures 2a and 2b, where  $\alpha(865) = +0.05$ . The resulting residual  $\alpha$ 's are presented in Table 1. The residual  $\alpha$ 's follow the expected pattern, i.e., Eq. (11), and in the first three bands are reduced to less than 1%. As mentioned above, this reduction is due to the increase in Rayleigh scattering with decreased  $\lambda_i$ . In fact, the Rayleigh optical thickness at 412 nm is approximately 12 times that at 765 nm, similar to the decrease in  $\alpha(412)$  compared to  $\alpha(765)$ . Note, however, that this method cannot even *detect* the error at  $\lambda_l$ .

The residual errors in Table 1 were added to the  $\rho_t$  pseudo data used to prepare Figure 1, and the Gordon and Wang correction algorithm was applied. The resulting error in  $t\rho_w$  at 443 nm is shown in Figure 3a. The error after this calibration adjustment is significantly reduced. In fact, it is similar to the error obtained when  $\alpha \approx +0.02$  in all bands. Figure 3b shows the further

improvement that would be possible if  $\alpha(\lambda_l)$  could be reduced to 0.025, half of its assumed initial value.

It is clear that the above method of calibration adjustment has the potential for reducing the effects of calibration errors; however, to effect the adjustment we need a method of determining the correct value of  $\varepsilon(\lambda_i, \lambda_l)$ . In addition, a method for reducing the error at the long wave band,  $\lambda_l$ , would further improve the retrieval of  $t\rho_w$  (Figure 3b).

*Gordon* [1997] studied the properties of a wide variety of aerosol models with both log-normal and power-law size distributions. That study suggested that measurement of  $\tau_a(\lambda_i)$ , for all  $\lambda_i$ , would allow a reasonable estimate of  $\varepsilon(\lambda_i, \lambda_l)$ . Figure 4 from *Gordon* [1997] provides examples showing the existence of a rough relationship between  $\tau_a(443)/\tau_a(865)$  and  $\varepsilon(443, 865)$  for several aerosol models. These models include nonabsorbing aerosols (open symbols) as well as weakly- and strongly-absorbing aerosols (solid symbols). Far from terrigenous and anthropogenic aerosol sources, where the aerosol over the ocean is locally generated, one expects nonabsorbing aerosols. Figure 4 suggests that  $\varepsilon(443, 865)$  in such cases can be estimated from  $\tau_a(443)/\tau_a(865)$  with an uncertainty  $\sim \pm 0.06$ , when it is near unity, i.e., for a pure maritime aerosol at high relative humidity [*Gordon and Wang*, 1994b]. Figures 2c and 2d show that if  $\varepsilon(443, 865)$  is known to within  $\pm 0.1$ , it should be possible to reduce  $|\alpha(443)|$  to  $\lesssim 0.01$ .

To reduce  $\alpha(\lambda_l)$  the full optical properties of the aerosol must be measured. *Wang and Gordon* [1993] have shown how to combine measurements of  $\tau_a$  and sky radiance over the oceans to obtain the aerosol phase function and single scattering albedo. Furthermore, the derived  $P_a$  and  $\omega_a$  can be inserted into the RTE to predict  $\rho_t$ . Predicting  $\rho_t$  in the visible requires measurement of  $\rho_w$ ; however, in the NIR  $\rho_w \approx 0$ , so  $\rho_t(\lambda_l)$  can be predicted without  $\rho_w$  measurements. *Gordon and Zhang* [1996] performed a complete sensitivity analysis of this procedure for predicting  $\rho_t$  and, as expected, under the most favorable conditions the error in the predicted  $\rho_t$  would be approximately the calibration uncertainty of the radiometer used in the measurement of the sky radiance, i.e., the accuracy of the procedure is limited by the accuracy of the surface-based radiometer, *not* the radiative transfer process. It is now possible to calibrate a radiometer relative to a standard lamp to within  $\pm 2.5\%$  [*Biggar, Slater and Gellman*, 1994], although it is believed that detector-based calibration could reduce the uncertainty to  $\pm 1\%$  [*Slater et al.*, 1996]. The *Gordon and Zhang* [1996] study suggests that the radiative transfer process would introduce an uncertainty in the prediction of  $\rho_t$  that is  $\lesssim \pm 1\%$  for error-free sky radiance measurements. Thus, assuming that the sky

radiance can be measured with an uncertainty of  $\pm 2.5\%$ , the *Gordon and Zhang* [1996] results suggest that the error in the predicted  $\rho_t$  should be  $\lesssim \pm 2.7\%$  in an RMS sense.

On the basis of the above discussion, we believe that it should be possible to reduce the  $\alpha(\lambda_i)$ 's to  $\lesssim 0.02 - 0.03$  in the NIR, and to significantly smaller values in the visible. Also, the residual  $\alpha(\lambda_i)$ 's will all have the same sign.

It is important to stress again that the calibration described here is *not* radiometric, but rather a calibration of the entire system — sensor *plus* algorithms. Also, since we use  $F_0$  to compute  $\rho_t$  in the procedure, the calibration is also relative to this quantity. An error in  $F_0(\lambda_i)$  will influence the resulting value of  $\alpha(\lambda_i)$ ; however, it will change in a very simple manner. The measured *radiance*  $L'_t$  is related to the true value  $L_t$  by  $L'_t = L_t(1 + \alpha_L)$ . This is converted to reflectance by multiplying by  $\pi/F_0 \cos \theta_0$ . If the extraterrestrial solar irradiance used in the conversion ( $F'_0$ ) is in error by a fraction  $\alpha_F$ , i.e.,  $F'_0 = F_0(1 + \alpha_F)$ , where  $F_0$  is the true value, then  $\rho'_t$  and  $\rho_t$  are related by

$$\rho'_t = \frac{(1 + \alpha_L)}{(1 + \alpha_F)} \rho_t \approx (1 + \alpha_L - \alpha_F) \rho_t.$$

Comparing with Eq. (2) we see that the value of  $\alpha(\lambda_i)$  resulting from the procedure is really  $\alpha_L(\lambda_i) - \alpha_F(\lambda_i)$ , i.e., it includes the effect of *both* the sensor radiometric calibration error and any error in the extraterrestrial the solar irradiance. Thus, our approach is pragmatic, no attempt is made to determine or understand the source of the error. The error in  $F_0$  (corrected for the variation in the earth-sun distance) is independent of time, and as long as the radiometric sensitivity of the instrument is independent of time (or its variation is monitored by other means), the algorithms should perform as suggested by the analysis provided for Figures 1 and 3.

Summarizing, by combining the correction algorithm, measurements of  $\rho_w$ , and an estimate of  $\varepsilon(\lambda_i, \lambda_l)$ , it is possible to reduce the  $F_0$ -sensor calibration error significantly in the visible, even with a rather large error ( $\sim 5\%$ ) at  $\lambda_l$ . *This alone could provide a calibration that will yield atmospheric correction to nearly the desired accuracy* (Figure 3a). Further reduction of the error requires reducing the uncertainty at  $\lambda_l$ . This can be accomplished by making atmospheric measurements sufficient to characterize the aerosol, and then predicting  $\rho_t(\lambda_l)$ . The final calibration accuracy at  $\lambda_l$  will be approximately the same as the accuracy of the surface-based radiometer used to characterize the aerosols.

## 5. Out-of-band response

We have implicitly assumed that the sensor's spectral response is a Dirac delta function. In reality, each spectral band will respond to radiance in a range of wavelengths, some even far from the nominal band width. If  $S_i(\lambda) d\lambda$  provides the electronic output (current or voltage) from the detector for unit input radiance in a narrow band  $d\lambda$  around  $\lambda_i$ , then the band radiance measured by the sensor in orbit will be

$$\langle L(\lambda) \rangle_{S_i} \equiv \frac{\int L(\lambda) S_i(\lambda) d\lambda}{\int S_i(\lambda) d\lambda},$$

i.e., the electronic output will be  $\propto \langle L(\lambda) \rangle_{S_i}$ . In an earlier paper [Gordon, 1995], I provided methodology for including the out-of-band response in the analysis of ocean color imagery, e.g., applying atmospheric correction to  $\langle L_t(\lambda) \rangle_{S_i}$ . It is straightforward to apply my analysis here, where the aerosol single scattering formulation of radiative transfer is believed to be valid. All that is necessary is to convert the radiance to reflectance through

$$\langle L(\lambda) \rangle_{S_i} = \frac{\cos \theta_0}{\pi} \langle \rho(\lambda) \rangle_{F_0 S_i},$$

where

$$\langle \rho(\lambda) \rangle_{F_0 S_i} \equiv \frac{\int \rho(\lambda) F_0(\lambda) S_i(\lambda) d\lambda}{\int F_0(\lambda) S_i(\lambda) d\lambda},$$

rewrite Eq. (4) for the band radiance  $\langle \rho(\lambda) \rangle_{F_0 S_i}$ , and then treat each term in a manner identical to Gordon [1995]. In the case of sensors with spectral bands that overlap a water vapor absorption band, e.g., SeaWiFS, the total column water vapor concentration is required. This can be obtained from the surface through sun photometry [Thome *et al.*, 1993].

## 6. Effect of multiple scattering and measurement error

In essence, the calibration adjustment used to reduce  $\alpha(\lambda_i)$  with respect to  $\alpha(\lambda_l)$  involves estimating  $\rho_t(\lambda_i)$  and then adjusting the sensor calibration so that it provides a value of  $\rho'_t(\lambda_i)$  in agreement with the estimate. The estimated  $\rho_t(\lambda_i)$  is given by

$$[\rho_t(\lambda_i)]_{Est} = \rho_r(\lambda_i) + t(\lambda_i)\rho_w(\lambda_i) + t(\lambda_i)\rho_{wc}(\lambda_i) + \varepsilon(\lambda_i, \lambda_l) \left[ \rho_t(\lambda_l) - \rho_r(\lambda_l) - t(\lambda_l)\rho_{wc}(\lambda_l) \right], \quad (12)$$

where, if  $\alpha(\lambda_l) = 0$ , the term in the square brackets is  $\rho_a(\lambda_l) + \rho_{ra}(\lambda_l)$ , and was called  $\rho_{aa}(\lambda_l)$  earlier (in the aerosol single-scattering approximation). This estimated  $\rho_t(\lambda_i)$  can be in error for several reasons: (1) error in the measured  $t(\lambda_i)\rho_w(\lambda_i)$  and/or  $t(\lambda_i)\rho_{wc}(\lambda_i)$ ; (2) error in  $\varepsilon(\lambda_i, \lambda_l)$  by

virtue of its estimation from  $\tau_a(\lambda_i)/\tau_a(\lambda_l)$ ; and error in the term in the square brackets [ $\alpha(\lambda_l) \neq 0$  and/or error in  $t(\lambda_l)\rho_{wc}(\lambda_l)$ ]. However, there is an additional error due to the fact that  $\epsilon(\lambda_i, \lambda_l)$  is a single-scattering quantity, i.e., it is not equal to

$$\epsilon_{MS}(\lambda_i, \lambda_l) \equiv \frac{\rho_a(\lambda_i) + \rho_{ra}(\lambda_i)}{\rho_a(\lambda_l) + \rho_{ra}(\lambda_l)},$$

which includes multiple scattering, and which must replace  $\epsilon(\lambda_i, \lambda_l)$  in Eq. (12) in order for the equation to provide the correct value of  $\rho_t(\lambda_i)$  in the absence of errors in any of the measured reflectances or in  $\rho_t(\lambda_l)$ . In fact, the difference between  $\epsilon(\lambda_i, \lambda_l)$  and  $\epsilon_{MS}(\lambda_i, \lambda_l)$  is at the core of the *Gordon and Wang* [1994b] atmospheric correction algorithm. Fortunately, given  $\epsilon(\lambda_i, \lambda_l)$  and  $\tau_a(\lambda_i)$ , computation of  $\epsilon_{MS}(\lambda_i, \lambda_l)$  is not difficult. One need only employ a nonabsorbing aerosol model (the aerosol expected at any suitable initialization site) that has a similar  $\epsilon(\lambda_i, \lambda_l)$ , and solve the radiative transfer equation to simulate the multiple scattering. As we are close to the single-scattering regime, error in the estimate of  $\epsilon_{MS}$  from  $\epsilon$  should be small.

With so many possible sources of error (four), it is difficult to assess the overall accuracy to be expected, as the errors may combine in many different ways. The approach we take here is to examine each error separately in the absence of the others. For simplicity we provide a numerical example. Consider a situation in which the aerosol at the initialization site is characterized by the *Shettle and Fenn* [1979] Maritime aerosol with 80% relative humidity (M80). Assume  $\theta_0 = 60^\circ$ , and the sensor views the ocean in the near-nadir direction. The oceanic site is oligotrophic with a pigment concentration (the sum of chlorophyll *a* and phaeophytin *a*)  $\sim 0.03$  mg/m<sup>3</sup>. The whitcap reflectance is characteristic of a wind speed of  $\sim 8$ -9 m/s, and possesses the spectral variation prescribed by *Frouin, Schwindling and Deschamps* [1996]. Under these conditions, the computed individual TOA reflectances (including multiple scattering) are provided in Table 2 for four spectral bands. The values provided for  $\rho_a + \rho_{ra}$  are for  $\tau_a(865) = 0.1$ . Given these values, we examined the error in the predicted  $\rho_t(\lambda_i)$  induced by a  $\pm 5\%$  error in  $t(\lambda_i)\rho_w(\lambda_i)$ , a  $\pm 50\%$  error in  $t(\lambda_i)\rho_{wc}(\lambda_i)$ , and a  $\pm 5\%$  (or  $\pm 2.5\%$ ) error in the measured  $\rho'_t(\lambda_l)$  ( $\alpha(\lambda_l) \neq 0$ ). The results of this exercise are provided in Table 3 for predictions made using both  $\epsilon(\lambda_i, \lambda_l)$  and  $\epsilon_{MS}(\lambda_i, \lambda_l)$  (the correct value). For the four bands in the chosen geometry with  $\tau_a(865) = 0.1$ ,  $\epsilon(\lambda_i, \lambda_l) = 1.124, 1.085, 1.027$ , and  $\epsilon_{MS}(\lambda_i, \lambda_l) = 1.247, 1.201$ , and  $1.054$ , respectively for  $\lambda_i = 443, 555$ , and  $765$  nm. Note that at 443 nm the difference between  $\epsilon_{MS}$  and  $\epsilon$  is  $\sim 0.1$ , i.e., a little larger than the expected uncertainty (Figure 4) in  $\epsilon(443, 865)$  derived from  $\tau_a(443)/\tau_a(865)$ , so the difference in two identical cases using  $\epsilon_{MS}$  and  $\epsilon$  provides an estimate of the error induced by error in  $\epsilon$  or  $\epsilon_{MS}$ . From Table 3 we see

that for a very clear atmosphere [ $\tau_a(\lambda_l) = 0$ ] error in  $\rho_{wc}(\lambda)$  produces very little error  $\rho_t(\lambda)$ . In contrast, error in  $\rho_w(\lambda)$  produces significant error in  $\rho_t$  at 443 nm ( $\sim 1\%$ ); however, notice that error in  $\rho_w(\lambda_i)$  produces a much smaller error in  $\rho_t(\lambda_i)$ . For  $\tau_a(\lambda_l) = 0.1$ , using the correct  $\epsilon_{MS}$ , error in  $\rho_w$ ,  $\rho_{wc}$ , and  $\rho_t(\lambda_l)$ , lead to errors in  $\rho_t(\lambda_i)$  that are similar to those with  $\tau_a(\lambda_l) = 0$ . When the incorrect  $\epsilon$  is used the errors are generally larger, and error in  $\rho'_t(\lambda_l)$ , especially when it is too small, can lead to rather large error in  $\rho_t(555)$ ; however, the effects at 443 nm are considerably less. As in the case when measurement errors are absent, typically the resulting  $\alpha(\lambda_i)$ 's all have the same sign (or when one has a different sign from the rest it has an insignificant magnitude). With the exception of the combination of a  $-5\%$  error in  $\rho_t(\lambda_l)$  and the incorrect  $\epsilon_{MS}$ ,  $\alpha(555)$  and  $\alpha(765)$  are similar to those in Table 1. In contrast,  $\alpha(443)$  is often larger, usually when there is error in  $\rho_w(443)$ . The message from Table 3 is clear: a high priority should be placed on reducing error in  $\rho_w(443)$ , and on finding the value of  $\epsilon_{MS}(\lambda_i, \lambda_l)$ . It is believed that  $\rho_w(\lambda_i)$  measurements can be carried out with an uncertainty  $< 5\%$ , indeed this is required to verify that the accuracy goal for  $\rho_w(443)$  is met. However, it would be possible to reduce further the effect of  $\rho_w$  uncertainty by choosing a mesotrophic initialization site, for which the value of  $\rho_w$  in the blue would be considerably reduced. As error in  $\rho_t(\lambda_l)$  can be important (especially in the presence of  $\epsilon_{MS}$  error), reduction of  $\alpha(\lambda_i)$  relative to  $\alpha(\lambda_l)$  should be effected *after* reduction  $\alpha(\lambda_l)$ . The entries in Table 3 for  $\alpha(865) = \pm 2.5\%$  show a concomitant improvement in  $\alpha(\lambda_i)$ .

As it is difficult to appreciate the effects of the residual errors shown in Table 3, we provide two examples of the quality of the atmospheric correction following a hypothetical initialization exercise. We assume that the atmosphere is very clear and use the  $\tau_a = 0$  residuals from Table 3. We ignore whitecaps error under the assumption that it will be  $\ll \pm 50\%$  (it is already almost insignificant at  $\pm 50\%$ ). The uncertainties due to  $\rho_w(443)$  and  $\rho_t(865)$  are assumed to add, i.e., the worst-case scenario. Figures 5a and 5b provide the resulting error in  $t(443)\rho_w(443)$  for  $\alpha(865) = +5\%$  and  $+2.5\%$ , respectively. In both cases the correction is within the desired  $\pm 0.002$  range. Comparing these figures with Figures 3a and 3b underscores the importance of reducing the uncertainty in the measurement of  $\rho_w(\lambda_i)$  if the measurements are carried out in oligotrophic waters.

## 7. Implementation Strategy

On the basis of Sections 3-6, we can enumerate the quantities that must be measured to implement the in-orbit calibration adjustment.

## 7A. Reduction of $\alpha(\lambda_i)$ relative to $\alpha(\lambda_l)$

In order to effect the reduction of  $\alpha(\lambda_i)$  relative to  $\alpha(\lambda_l)$ , i.e., Eq. (11), we require  $t(\lambda_i)$  and  $\rho_w(\lambda_i)$  to provide  $t\rho_w$ ,  $\tau_a(\lambda_i)/\tau_a(\lambda_l)$  to provide  $\varepsilon(\lambda_i, \lambda_l)$ , surface atmospheric pressure ( $P$ ) to provide  $\rho_r(\lambda_i)$ , and an assessment of  $\rho_{wc}(\lambda_i)$  if whitecaps are present. These quantities must be measured in an oceanic area for which  $\tau_a(\lambda)$  in the visible is  $\lesssim 0.10$ . The water-leaving reflectance  $\rho_w(\lambda)$  should be horizontally uniform (or its variability assessed) over the scale of a few pixels around the measurement location. The water-leaving reflectance is deduced from measurement of  $\rho_u$ , the subsurface upwelled reflectance distribution. With the exception of  $t(\lambda_i)$ , the instrumentation required to effect these measurements is described in *Clark et al.* [1997]. In the clear atmospheres required for this exercise, computation of  $t(\lambda_i)$  is easily effected [ *Yang and Gordon, 1997* ].

The desirable attributes of the calibration initialization site are (1) a very clear atmosphere ( $\tau_a \lesssim 0.1$  in the visible), (2) horizontally uniform  $\rho_w$  over spatial scales of a few pixels (a few km), and (3) mesotrophic waters to reduce the effect of  $\rho_w$  measurement error in the blue. It is usually not possible to find a site possessing all three attributes. For example, the central gyres of the oceans usually possess attributes (1) and (2), except under situations when desert dust is transported to them by the winds. However, they become mesotrophic only episodically, e.g., during spring bloom conditions. Mesotrophic conditions often occur closer to land (shelf and slope regions); however, in these regions  $\tau_a(\lambda)$  is not likely to be low. Because assessing the aerosol contribution under high aerosol loads is difficult, we drop attribute (3) in favor of (1) and (2). An apparently suitable site that possess attributes (1) and (2) is windward ( $\sim 100$  km) of the Hawaiian Islands. This site is logistically attractive (see Section 8) and should meet the requirements; however, the accuracy requirement on the  $\rho_w$  measurement will be challenging.

## 7B. Reduction of $\alpha(\lambda_l)$

In order to effect a reduction of  $\alpha(\lambda_l)$ , measurement of the normalized sky radiance  $\rho_{sky}$ , and aerosol optical thickness at  $\lambda_l$ , either at sea or from a small island, are required to utilize the methods of *Gordon and Zhang* [1996]. *Clark et al.* [1997] describe instrumentation currently available for such measurements. These measurements should be made close to the time of the satellite overpass; however, there are geometrical constraints. Using the *Gordon and Zhang* [1996]  $\rho_t$  inversion-prediction approach, the aerosol scattering phase function can be retrieved only for

scattering angles  $\Theta$  for which the direct solar beam can be singly scattered into the sky radiometer. The maximum angle for which this is possible,  $\Theta_{\text{Max}}$ , is  $\theta_0 + 90^\circ$ , and so  $P_a(\Theta, \lambda)$  can be determined only for  $0 \leq \Theta < \Theta_{\text{Max}} = \theta_0 + 90^\circ$ . As  $\Theta_{\text{Max}}$  corresponds to viewing in the horizontal direction, practically, the maximum  $\Theta$  will be  $\sim 5^\circ$  less than  $\Theta_{\text{Max}}$ . Accurate predictions of the TOA reflectance  $\rho_t$  are possible only for those directions for which the solar beam can be singly scattered into the sensor through a scattering angle  $< \Theta_{\text{Max}}$ . For nadir viewing, the required scattering angle is  $\Theta_N = 180^\circ - \theta_0$ . For viewing at the scan edge (taken here to be  $\theta_v = 45^\circ$ ,  $\phi_v - \phi_0 = 90^\circ$ ), the required scattering angle  $\Theta_E$  is given by  $\cos \Theta_E = -0.707 \cos \theta_0$ . Figure 6 provides  $\Theta_{\text{Max}}$ ,  $\Theta_N$ , and  $\Theta_E$  as functions of  $\theta_0$ . Noting that  $\Theta$  must be  $< \Theta_{\text{Max}}$  to effect a vicarious calibration, Figure 6 shows that this is possible only for  $\theta_0 \gtrsim 35^\circ$  at the scan edge, and  $\theta_0 > 45^\circ$  at the scan center (nadir viewing). When the practical limit on  $\Theta_{\text{Max}}$  is considered ( $\Theta_{\text{Max}}$  reduced by  $\sim 5^\circ$ ), we find that  $\theta_0 \gtrsim 47^\circ$  at the scan center, and  $\theta_0 \gtrsim 38^\circ$  near the scan edge.

These geometrical constraints, coupled with the fact that ocean color sensors are typically in orbits for which the satellite overpass is within 1.5 hr of local noon, generally means that for simultaneous surface and satellite measurements to be possible in the northern hemisphere, the measurements must be carried out at mid latitudes near the winter solstice. Note that, although the reduction of  $\alpha(\lambda_l)$  will be attempted at sea simultaneously with the reduction of  $\alpha(\lambda_i)$ ,  $\lambda_i < \lambda_l$ , it can be carried out in a separate experiment at a different location and time if necessary, i.e., independently of the reduction of  $\alpha(\lambda_i)$ ,  $\lambda_i < \lambda_l$ .

Although several sites are under consideration for an independent  $\alpha(\lambda_l)$  reduction exercise, one that appears to possess the desirable attributes is the area surrounding the Dry Tortugas ( $\sim 24^\circ 38' \text{N}$ ,  $82^\circ 53' \text{W}$ ) in the Southern Gulf of Mexico. Presently, this site is part of the AERONET network [Holben *et al.*, 1997] and is equipped with instrumentation for measuring  $\rho_{\text{sky}}(\lambda)$  and  $\tau_a(\lambda)$ . The island is sufficiently small that no corrections for its perturbation to the sky radiance should be required [Yang, Gordon and Zhang, 1995]. Although the waters in the vicinity of the island are shallow ( $\sim$  few meters), the strong absorption of liquid water at  $\lambda_l$  ( $\sim 5 \text{ m}^{-1}$  at 865 nm) should prevent any bottom contribution to  $\rho_w(\lambda_l)$ , so the assumption that  $\rho_w(\lambda_l) = 0$  should still be valid. (This can be verified by direct measurements.) During the winter, the passage of cold fronts at  $\sim 5$ -10 day intervals produce exceptionally clear atmospheres ( $\tau_a$  as low as 0.04 at 670 nm). In this season, solar zenith angles  $\sim 40^\circ - 50^\circ$  occur near solar noon, the approximate time of a SeaWiFS overpass. Solar zenith angles at the time of a MODIS overpass ( $\sim 1.5$  hours before local noon)

can be as large as  $56^\circ$  (Figure 7). Noting that in practice we require  $\theta_0 \gtrsim 47^\circ$  at the scan center and  $38^\circ$  at the scan edge, we see that in the case of MODIS, vicarious calibration is possible for a considerable number of days around the solstice irrespective of the scan angle. In contrast, for SeaWiFS (equator crossing at local noon) calibration can be effected at the scan center only near the solstice, but near the scan edge, it could be effected for several weeks on either side of the solstice. In the year 2000 a second MODIS instrument is planned to be launched with an equator crossing 1.5 hours after local noon. Figure 7 shows that the above comments regarding SeaWiFS would apply equally well to this second MODIS.

Our definition of the scan edge ( $45^\circ$  viewing angle) is somewhat arbitrary. In fact, SeaWiFS will acquire data for  $\theta_v$  as large as  $58^\circ$  (although the atmospheric correction for  $\theta_v \gtrsim 45^\circ$  is not expected to be accurate). At  $\theta_v = 58^\circ$  the minimum  $\theta_0$  is  $\sim 30^\circ$ , and this vicarious calibration technique could be extended to about 75 days on either side of the solstice.

Finally, it should be noted that the *Gordon and Zhang* [1996] technique works best when  $\theta_0$  is large, e.g.,  $60^\circ$ , in which case one need guess at only a small portion of the scattering phase function at large angles. One way to achieve this is to measure the sky radiance at large  $\theta_0$  and use this data to retrieve the scattering phase function, and then predict  $\rho_t$  later in the day when the satellite overpass occurs. This would allow its application in situations where  $\Theta_{\text{Max}} < \Theta_N$  or  $\Theta_E$ , e.g., during at-sea exercises for reducing  $\alpha(\lambda_t)$  relative to  $\alpha(\lambda_l)$ , should such exercises occur during summer. For SeaWiFS the sky radiance to be inverted would have to be acquired  $\sim 1.5 - 2$  hours prior to the overpass at the Dry Tortugas site. As the AERONET sky radiometer/photometer operates in a nearly continuous mode, any change in the aerosol optical properties over the 1.5–2 hour period should be evident in the aerosol optical thickness spectral data. *Gordon and Zhang* [1996] provide examples of the expected accuracy in the predicted  $\rho_t(\lambda_l)$  under conditions for which  $\rho_{\text{sky}}$  is obtained when  $\theta_0 = 60^\circ$ , but  $\rho_t$  is predicted for  $\theta_0 = 45^\circ$  and  $50^\circ$ .

The basic approach to the reduction of  $\alpha(\lambda_l)$  will be to continuously acquire sky radiance data throughout the winter months and use only those data acquired under optimum conditions to predict  $\rho_t(\lambda_l)$ . The main challenge will be the radiometric calibration of the sky radiometer. Presently, these radiometers are calibrated using an integrating sphere at Goddard Space Flight Center. This sphere has been part of the SeaWiFS Intercalibration Round-Robin Experiments (SIRREX) [*Johnson et al.*, 1996; *Mueller*, 1993; *Mueller et al.*, 1994; *Mueller et al.*, 1996], and as such the sky radiometer is calibrated with the same standards and protocols as the radiometers

used to measure  $\rho_w$  in Subsection 7A. However, maintaining the calibration of such unattended instruments is difficult.

### 7C. Summary of Required Measurements

The surface measurements required for the two vicarious calibration exercises described in this section are summarized in Table 4. Note that both exercises can be carried out at the same location if desired; however, it is not necessary. It is important to note that effecting the reduction of  $\alpha(\lambda_i)$  in the summer, when  $\theta_0$  is small at the time of the sensor overpass, will require that  $\rho_{sky}$  is measured several hours prior to the overpass and that the stability of the atmosphere be monitored continuously between the times of the measurement and the overpass. Column  $H_2O$  is required only for sensors for which  $S_i(\lambda)$  overlaps water vapor absorption bands.

### 8. Maintenance of Calibration

The strategy of maintaining the sensor calibration involves utilizing the on-board solar diffusers to monitor short-term variations in the calibration. However, as the reflectance of such diffusers may gradually decay, it is necessary to assess the long-term stability by other means. The strategy we plan to monitor long-term variations is the use of an unattended measurement of  $\rho_w$  at a single site where atmospheric correction of the satellite data is simple enough that it will not introduce significant error in the retrieval of  $\rho_w$ . Comparison of the satellite-retrieved and directly-measured  $\rho_w$  over long time periods ( $\sim$  several months to years) will provide a measure of the long-term variation in the calibration of the sensor. In addition, periodic observation of the moon can also provide a measure of the long-term stability (SeaWiFS) [Kieffer and Wildey, 1996].

To provide knowledge of the long-term stability of the calibration as well as a quality measure of the performance of the sensor and the algorithms, Clark has developed a marine optical buoy system (MOBY) for continuous and unattended measurement of  $\rho_w(\lambda)$  near the nadir direction (radiance exciting the ocean propagating toward the zenith). A description of this system and its planned operation is provided in Clark *et al.* [1997]. Briefly, this buoy is moored  $\sim$  11.3 nautical miles east of the island of Lanai in the Hawaiian chain, and provides nearly real time estimates of  $\rho_w(\lambda)$  near the nadir direction on a continuous basis. As the sensor will not usually be looking at the site in the nadir direction, corrections to the radiance are required to account for the bidirectional

effects of the upwelling subsurface spectral radiance [Morel and Gentili, 1991; Morel and Gentili, 1993; Morel and Gentili, 1996; Morel, Voss and Gentili, 1995]. The magnitude of these effects can be assessed and corrected through a combination of models and direct measurements of the angular distribution of upwelling subsurface radiance in the vicinity of the site under a variety of conditions [Voss, 1989]. Although this data will be of somewhat lower quality than ship-acquired  $\rho_w$  data it should be sufficiently accurate for monitoring the long-term performance of the instrument.

## 9. Concluding remarks

As described in the introduction, it is not possible to calibrate ocean color sensors in the laboratory with the required accuracy prior to launch. In this paper we have summarized methodology to effect in-orbit calibration adjustment of ocean color sensors with an accuracy sufficient to provide  $\rho_w$  with the required uncertainty. The “vicarious” calibration uses a combination of surface measurements and the atmospheric radiative transfer process to predict the values of the spectral radiance that the sensor is measuring. As such, this work is an extension (to the ocean) of the methodology used earlier to calibrate principally land-viewing sensors [Fraser and Kaufman, 1986; Koepke, 1982; Slater *et al.*, 1987; Slater *et al.*, 1996].

Conditions are chosen (very clear atmospheres with nonabsorbing aerosols) so that the radiative transfer process introduces very little error into the estimates, i.e., conditions under which the atmospheric correction algorithm should provide excellent retrievals of  $\rho_w$ , and for which error in sensor calibration are particularly evident (especially in the blue).

The calibration adjustment is in three parts. First, the calibration error in the visible bands is reduced relative to that at  $\lambda_l$  by using surface measurements of  $\rho_w(\lambda)$ ,  $\tau_a(\lambda)$ , and  $\rho_{wc}(\lambda)$ . This in itself can provide a calibration that enables retrieval of  $\rho_w(\lambda)$  from  $\rho_t(\lambda)$  with nearly the required accuracy (Figure 3). Next, the error at  $\lambda_l$  is reduced by making measurements of the sky radiance and  $\tau_a$  from a ship, or an island location, simultaneously (or contemporaneously) with the satellite overpass. Inversion of the sky radiance provides the radiative properties of the aerosol, and these can be used to estimate the desired  $\rho_t(\lambda_l)$  [Gordon and Zhang, 1996]. Finally, as solar diffusers on SeaWiFS and MODIS provide the capability of monitoring the short-term radiometric sensitivity,  $\rho_w(\lambda)$  is continuously measured at a fixed location and compared with its retrieved counterpart to monitor variations in the long-term radiometric sensitivity of the sensor.

## References

- Biggar, S. F., P. N. Slater and D. I. Gellman, Uncertainties in the in-flight calibration of sensors with reference to measured ground sites in the 0.4 to 1.1  $\mu\text{m}$  range, *Remote Sensing of Environment*, 48, 245–252, 1994.
- Clark, D. K., H. R. Gordon, K. J. Voss, Y. Ge, W. Broenkow and C. Trees, 1997, Validation of Atmospheric Correction over the Oceans, *Jour. Geophys. Res.*, (In press).
- Ding, K. and H. R. Gordon, Analysis of the influence of O<sub>2</sub> A-band absorption on atmospheric correction of ocean color imagery, *Applied Optics*, 34, 2068–2080, 1995.
- Evans, R. H. and H. R. Gordon, CZCS 'System Calibration.' A retrospective examination, *Jour. Geophys. Res.*, 99C, 7293–7307, 1994.
- Fraser, R. S. and Y. J. Kaufman, Calibration of satellite sensors after launch, *Applied Optics*, 25, 1177–1185, 1986.
- Frouin, R., M. Schwindling and P. Y. Deschamps, Spectral reflectance of sea foam in the visible and near-infrared: In-situ measurements and implications for remote sensing of ocean color and aerosols, *Jour. Geophys. Res.*, 101C, 14,361–14,371, 1996.
- Gordon, H. R., Calibration Requirements and Methodology for Remote Sensors Viewing the Oceans in the Visible, *Remote Sensing of Environment*, 22, 103–126, 1987.
- Gordon, H. R., Remote sensing of ocean color: a methodology for dealing with broad spectral bands and significant out-of-band response, *Applied Optics*, 34, 8363–8374, 1995.
- Gordon, H. R., 1997, Atmospheric Correction of Ocean Color Imagery in the Earth Observing System Era, *Jour. Geophys. Res.*, (In press).
- Gordon, H. R., J. W. Brown and R. H. Evans, Exact Rayleigh Scattering Calculations for use with the Nimbus-7 Coastal Zone Color Scanner, *Applied Optics*, 27, 862–871, 1988.

- Gordon, H. R. and A. Y. Morel, *Remote Assessment of Ocean Color for Interpretation of Satellite Visible Imagery: A Review*, Springer-Verlag, New York, 1983, 114 pp.
- Gordon, H. R. and M. Wang, Influence of Oceanic Whitecaps on Atmospheric Correction of SeaWiFS, *Applied Optics*, 33, 7754–7763, 1994a.
- Gordon, H. R. and M. Wang, Retrieval of water-leaving radiance and aerosol optical thickness over the oceans with SeaWiFS: A preliminary algorithm, *Applied Optics*, 33, 443–452, 1994b.
- Gordon, H. R. and T. Zhang, How well can radiance reflected from the ocean-atmosphere system be predicted from measurements at the sea surface?, *Applied Optics*, 35, 6527–6543, 1996.
- Holben, B. N., T. F. Eck, I. Slutsker, D. Tanre, J. P. Buis, A. Setzer, E. Vermote, J. Reagan, Y. Kaufman, T. Nakajima, F. Lavenu and I. Jankowiak, 1997, Automatic Sun and Sky Scanning Radiometer System for Network Aerosol Monitoring, *Remote Sensing of Environment* (In press) .
- Hooker, S. B., W. E. Esaias, G. C. Feldman, W. W. Gregg and C. R. McClain, *SeaWiFS Technical Report Series: Volume 1, An Overview of SeaWiFS and Ocean Color*, NASA, Greenbelt, MD, Technical Memorandum 104566, July 1992.
- Johnson, B. C., S. S. Bruce, E. A. Early, J. M. Houston, T. R. O'Brian, A. Thompson, S. B. Hooker and J. L. Mueller, *SeaWiFS Technical Report Series: Volume 37, The Fourth SeaWiFS Intercalibration Round-Robin Experiment, SIRREX-4, May 1995*, NASA, Greenbelt, MD, Technical Memorandum 104566, May 1996.
- Kieffer, H. H. and R. L. Wildey, Establishing the Moon as a Spectral Radiance Standard, *Jour. Atmos. Oceanic Tech.*, 13, 360–375, 1996.
- Koepke, P., Vicarious Satellite Calibration in the Solar Spectral Range by Means of Calculated Radiances and its Application to Meteosat, *Applied Optics*, 21, 2845–2854, 1982.

- Korotaev, G. K., S. M. Sakerin, A. M. Ignatov, L. L. Stowe and E. P. McClain, Sun-Photometer Observations of Aerosol Optical Thickness over the North Atlantic from a Soviet Research Vessel for Validation of Satellite Measurements, *Jour. Atmos. Oceanic Technol.*, 10, 725–735, 1993.
- Moore, K. D., K. J. Voss and H. R. Gordon, 1997, Spectral Reflectance of Whitecaps: Fractional Coverage and the Augmented Spectral Reflectance Contribution to Water-Leaving Radiance, *Jour. Geophys. Res.*, (Submitted).
- Morel, A. and B. Gentili, Diffuse reflectance of oceanic waters: its dependence on Sun angle as influenced by the molecular scattering contribution, *Applied Optics*, 30, 4427–4438, 1991.
- Morel, A. and B. Gentili, Diffuse reflectance of oceanic waters. II. Bidirectional aspects, *Applied Optics*, 32, 6864–6879, 1993.
- Morel, A. and B. Gentili, Diffuse reflectance of oceanic waters. III. Implication of bidirectionality for the remote sensing problem, *Applied Optics*, 35, 4850–4862, 1996.
- Morel, A., K. J. Voss and B. Gentili, Bidirectional reflectance of oceanic waters: A comparison of modeled and measured upward radiance fields, *Jour. Geophys. Res.*, 100C, 13,143–13,150, 1995.
- Mueller, J. L., *SeaWiFS Technical Report Series: Volume 14, The First SeaWiFS Intercalibration Round-Robin Experiment, SIRREX-1, July 1992*, NASA, Greenbelt, MD, Technical Memorandum 104566, September 1993.
- Mueller, J. L., B. C. Johnson, C. L. Cromer, J. W. Cooper, J. T. McLean, S. B. Hooker and T. L. Westphal, *SeaWiFS Technical Report Series: Volume 16, The Second SeaWiFS Intercalibration Round-Robin Experiment, SIRREX-2, June 1993*, NASA, Greenbelt, MD, Technical Memorandum 104566, May 1994.

- Mueller, J. L., B. C. Johnson, C. L. Cromer, S. B. Hooker, J. T. McLean and S. F. Biggar, *SeaWiFS Technical Report Series: Volume 34, The Third SeaWiFS Intercalibration Round-Robin Experiment, SIRREX-3, September 1994*, NASA, Greenbelt, MD, Technical Memorandum 104566, March 1996.
- Reddy, P. J., F. W. Kreiner, J. J. Deluisi and Y. Kim, Aerosol Optical Depths Over the Atlantic Derived From Shipboard Sunphotometer Observations During the 1988 Global Change Expedition, *Global Biogeochemical Cycles*, 4, 225–240, 1990.
- Salomonson, V. V., W. L. Barnes, P. W. Maymon, H. E. Montgomery and H. Ostrow, MODIS: Advanced Facility Instrument for Studies of the Earth as a System, *IEEE Geosci. Rem. Sens.*, 27, 145–152, 1989.
- Shettle, E. P. and R. W. Fenn, Models for the Aerosols of the Lower Atmosphere and the Effects of Humidity Variations on Their Optical Properties, Air Force Geophysics Laboratory, Hanscomb AFB, MA 01731, AFGL-TR-79-0214, 1979.
- Slater, P. N., S. F. Biggar, R. G. Holm, R. D. Jackson, Y. Mao, M. S. Moran, J. M. Palmer and B. Yuan, Reflectance- and Radiance-Based Methods for the In-Flight Absolute Calibration of Multispectral Sensors, *Remote Sensing of Environment*, 22, 11–37, 1987.
- Slater, P. N., S. F. Biggar, K. J. Thome, D. I. Gellman and P. R. Spyak, Vicarious radiometric calibration of EOS sensors, *Jour. Atmos. Oceanic Tech.*, 13, 349–359, 1996.
- Thome, K. J., M. W. Smith, J. M. Palmer and J. A. Reagan, Method and instrument for retrieving total columnar water vapor from solar transmittance, *Proceedings, Society of Photo-Optical Instrumentation Engineers*, 1968, 856–861, 1993.
- Villevalde, Y. V., A. V. Smirnov, N. T. O'Neill, S. P. Smyshlyaev and V. V. Yakovlev, Measurement of Aerosol Optical Depth in the Pacific Ocean and North Atlantic, *Jour. Geophys. Res.*, 99D, 20983–20988, 1994.
- Voss, K. J., Electro-optic Camera System for Measurement of the Underwater Radiance Distribution, *Optical Engineering*, 28, 241–247, 1989.

Wang, M. and H. R. Gordon, Retrieval of the Columnar Aerosol Phase Function and Single Scattering Albedo from Sky Radiance over the Ocean: Simulations, *Applied Optics*, 32, 4598–4609, 1993.

Wang, M. and H. R. Gordon, A Simple, Moderately Accurate, Atmospheric Correction Algorithm for SeaWiFS, *Remote Sensing of Environment*, 50, 231–239, 1994.

Yang, H. and H. R. Gordon, 1997 , Remote sensing of ocean color: Assessment of the water-leaving radiance bidirectional effects on the atmospheric diffuse transmittance, *Applied Optics*, (Submitted).

Yang, H., H. R. Gordon and T. Zhang, Island perturbation to the sky radiance over the ocean: Simulations, *Applied Optics*, 34, 8354–8362, 1995.

**Table 1:** Values of  $\alpha(\lambda_i)$  required to produce a nearly correct  $\varepsilon(\lambda_i, \lambda_i)$  for the examples in Figures 2a and 2b.

$\lambda_i$ (nm)	$\alpha(\lambda_i)$
412	0.003
443	0.005
490	0.008
520	0.01
550	0.015
670	0.02
765	0.03

**Table 2:** Reflectance for M80 model near nadir.

( $\theta_0 = 60^\circ$ ,  $\tau_a(865) = 0.1$ ,  $\lambda$  in nm)

$\lambda$	$\rho_r(\lambda)$	$t\rho_w(\lambda)$	$t\rho_{wc}(\lambda)$	$\rho_a(\lambda) + \rho_{ra}(\lambda)$
443	0.11948	0.02667	0.00140	0.00939
555	0.04923	0.00348	0.00174	0.00905
765	0.01331	0	0.00173	0.00793
443	0.00806	0	0.00156	0.00752

**Table 3: Summary of residual errors  $\alpha(\lambda_i)$  after calibration adjustment.**

$\tau_a$	$\delta\rho_w(\lambda)$ (%)	$\delta\rho_{wc}(\lambda)$ (%)	$\varepsilon$	$\varepsilon_{MS}$	$\alpha(443)$ (%)	$\alpha(555)$ (%)	$\alpha(765)$ (%)	$\alpha(865)$ (%)
0	0	0			0	0	0	0
0	0	0			$\pm 0.18$	$\pm 0.48$	$\pm 1.64$	$\pm 2.5$
0	0	0			$\pm 0.38$	$\pm 0.97$	$\pm 3.27$	$\pm 5.0$
0	$\pm 5$	0			$\pm 0.90$	$\pm 0.32$	0	0
0	0	$\pm 50$			$\mp 0.14$	$\pm 0.02$	$\pm 0.43$	0
0.1	0	0		✓	0	0	0	0
0.1	0	0		✓	$\pm 0.34$	$\pm 0.81$	$\pm 1.97$	$\pm 2.5$
0.1	0	0		✓	$\pm 0.68$	$\pm 1.62$	$\pm 3.93$	$\pm 5.0$
0.1	$\pm 5$	0		✓	$\pm 0.85$	$\pm 0.27$	0	0
0.1	0	$\pm 50$		✓	$\pm 0.17$	$\pm 0.11$	$\pm 0.19$	0
0.1	0	0	✓		-0.59	-1.38	-0.85	0
0.1	0	0	✓		-0.28	-0.64	+1.07	+2.5
0.1	0	0	✓		+0.02	+0.09	+2.99	+5.0
0.1	0	0	✓		-0.90	-2.11	-2.77	-2.5
0.1	0	0	✓		-1.21	-2.84	-4.68	-5.0
0.1	+5	0	✓		+0.26	-1.10	-0.85	0
0.1	-5	0	✓		-1.44	-1.65	-0.85	0
0.1	0	+50	✓		-0.70	-1.34	-0.57	0
0.1	0	-50	✓		-0.48	-1.41	-1.12	0

**Table 4: Measurements required for vicarious calibration.**

Reduction of $\alpha(\lambda_i)$ , $\lambda_i < \lambda_l$	Reduction of $\alpha(\lambda_l)$
$\rho_u(\lambda_i)$ angular distribution	$\rho_{sky}(\lambda_l)$
$\tau_a(\lambda_i)/\tau_a(\lambda_l)$	$\tau_a(\lambda_l)$
$\rho_{wc}(\lambda_i)$	
Assess horizontal variation of $\rho_w(\lambda_i)$	
Column H <sub>2</sub> O	Column H <sub>2</sub> O

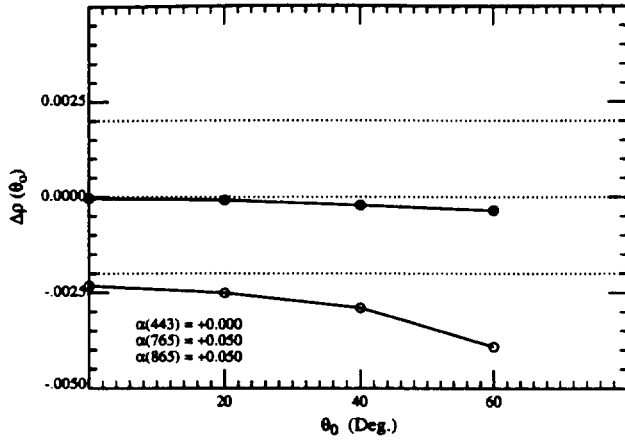


Figure 1a. Error in the retrieved  $t(443)\rho_w(443)$  for viewing near the edge of the scan with a Maritime aerosol at RH = 80% as a function of the solar zenith angle with  $\tau_a(865) = 0.2$  and calibration errors  $\alpha(443)$ ,  $\alpha(765)$ , and  $\alpha(865)$  in Eq. (2) (open circles). Solid circles are for  $\alpha(\lambda_i) = 0$  for all  $\lambda_i$ .

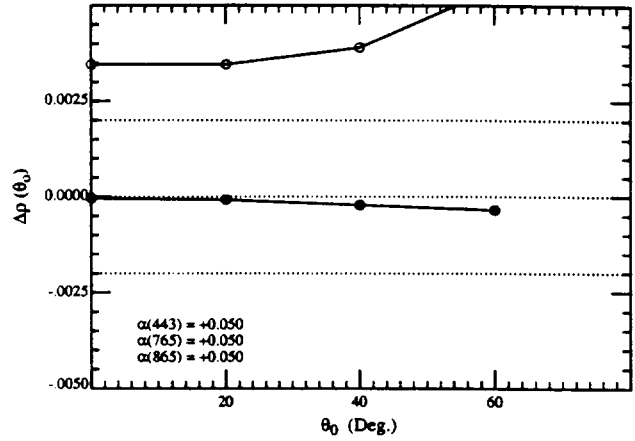


Figure 1b. Error in the retrieved  $t(443)\rho_w(443)$  for viewing near the edge of the scan with a Maritime aerosol at RH = 80% as a function of the solar zenith angle with  $\tau_a(865) = 0.2$  and calibration errors  $\alpha(443)$ ,  $\alpha(765)$ , and  $\alpha(865)$  in Eq. (2) (open circles). Solid circles are for  $\alpha(\lambda_i) = 0$  for all  $\lambda_i$ .

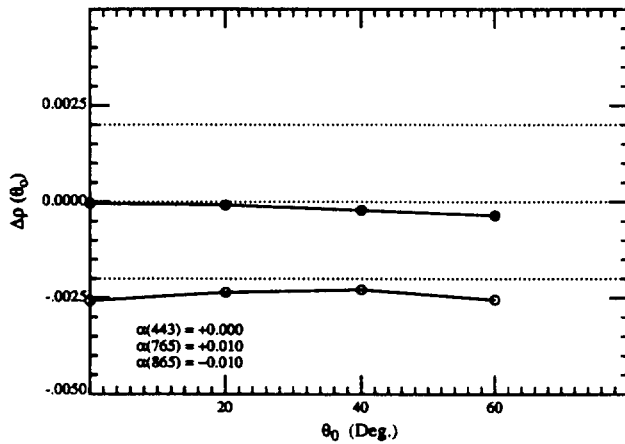


Figure 1c. Error in the retrieved  $t(443)\rho_w(443)$  for viewing near the edge of the scan with a Maritime aerosol at RH = 80% as a function of the solar zenith angle with  $\tau_a(865) = 0.2$  and calibration errors  $\alpha(443)$ ,  $\alpha(765)$ , and  $\alpha(865)$  in Eq. (2) (open circles). Solid circles are for  $\alpha(\lambda_i) = 0$  for all  $\lambda_i$ .

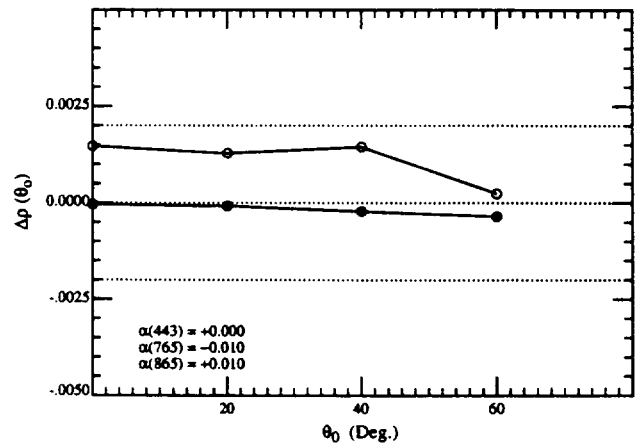


Figure 1d. Error in the retrieved  $t(443)\rho_w(443)$  for viewing near the edge of the scan with a Maritime aerosol at RH = 80% as a function of the solar zenith angle with  $\tau_a(865) = 0.2$  and calibration errors  $\alpha(443)$ ,  $\alpha(765)$ , and  $\alpha(865)$  in Eq. (2) (open circles). Solid circles are for  $\alpha(\lambda_i) = 0$  for all  $\lambda_i$ .

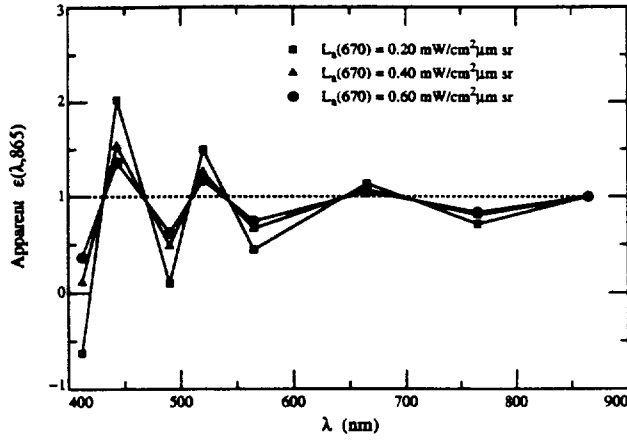


Figure 2a. Apparent value of  $\epsilon(\lambda, 865)$  for three values of  $L_s(670)$ .  $\alpha(\lambda)$  alternates in sign from band to band and  $|\alpha(\lambda)| = 0.05$ .

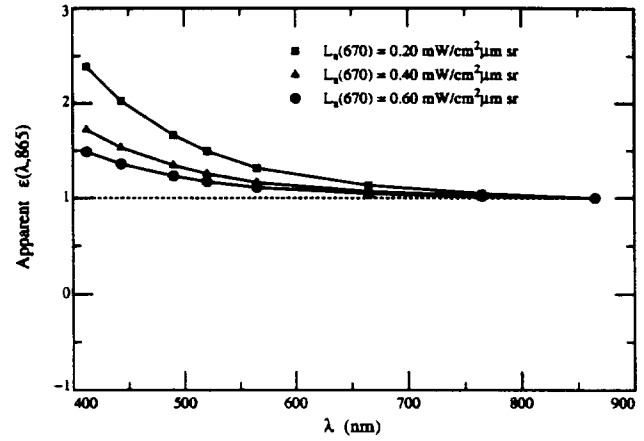


Figure 2b. Apparent value of  $\epsilon(\lambda, 865)$  for three values of  $L_s(670)$ .  $\alpha(\lambda) = 0.05$  for all bands.

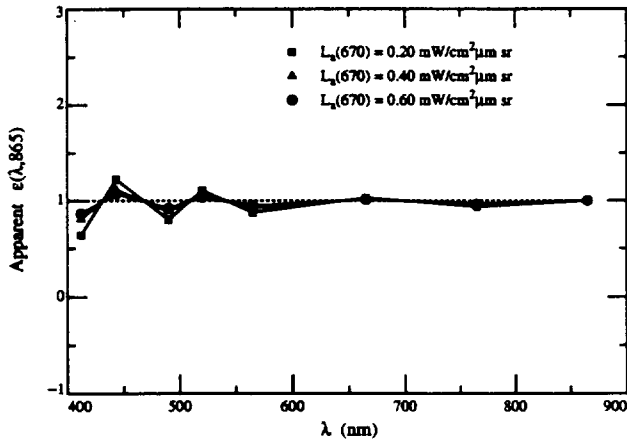


Figure 2c. Apparent value of  $\epsilon(\lambda, 865)$  for three values of  $L_s(670)$ .  $\alpha(\lambda)$  alternates in sign from band to band and  $|\alpha(\lambda)| = 0.01$ .

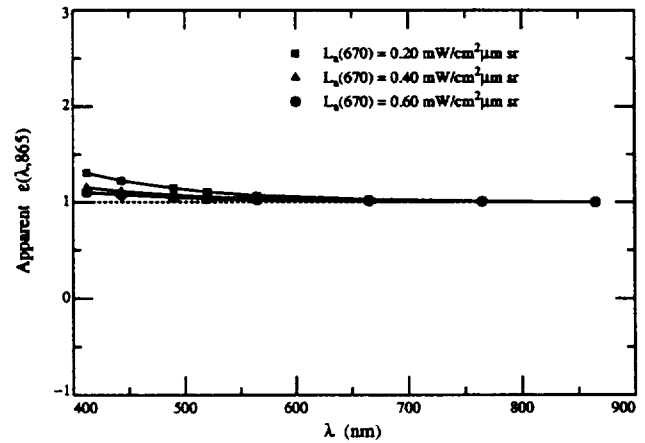


Figure 2d. Apparent value of  $\epsilon(\lambda, 865)$  for three values of  $L_s(670)$ .  $\alpha(\lambda) = 0.01$  for all bands.

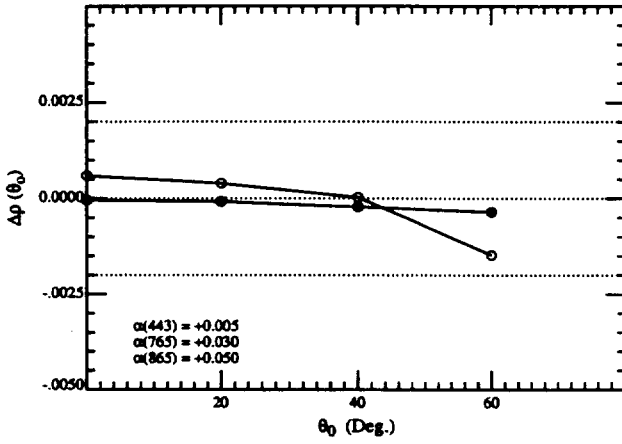


Figure 3a. Error in the retrieved  $t(443)\rho_w(443)$  for viewing near the edge of the scan with a Maritime aerosol at RH = 80% as a function of the solar zenith angle with  $\tau_a(865) = 0.2$  and calibration errors  $\alpha(443)$ ,  $\alpha(765)$ , and  $\alpha(865)$  in Eq. (2) (open circles). Solid circles are for  $\alpha(\lambda_i) = 0$  for all  $\lambda_i$ .

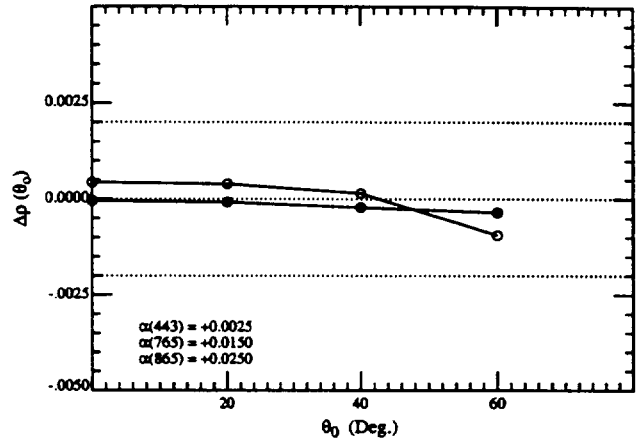


Figure 3b. Error in the retrieved  $t(443)\rho_w(443)$  for viewing near the edge of the scan with a Maritime aerosol at RH = 80% as a function of the solar zenith angle with  $\tau_a(865) = 0.2$  and calibration errors  $\alpha(443)$ ,  $\alpha(765)$ , and  $\alpha(865)$  in Eq. (2) (open circles). Solid circles are for  $\alpha(\lambda_i) = 0$  for all  $\lambda_i$ .

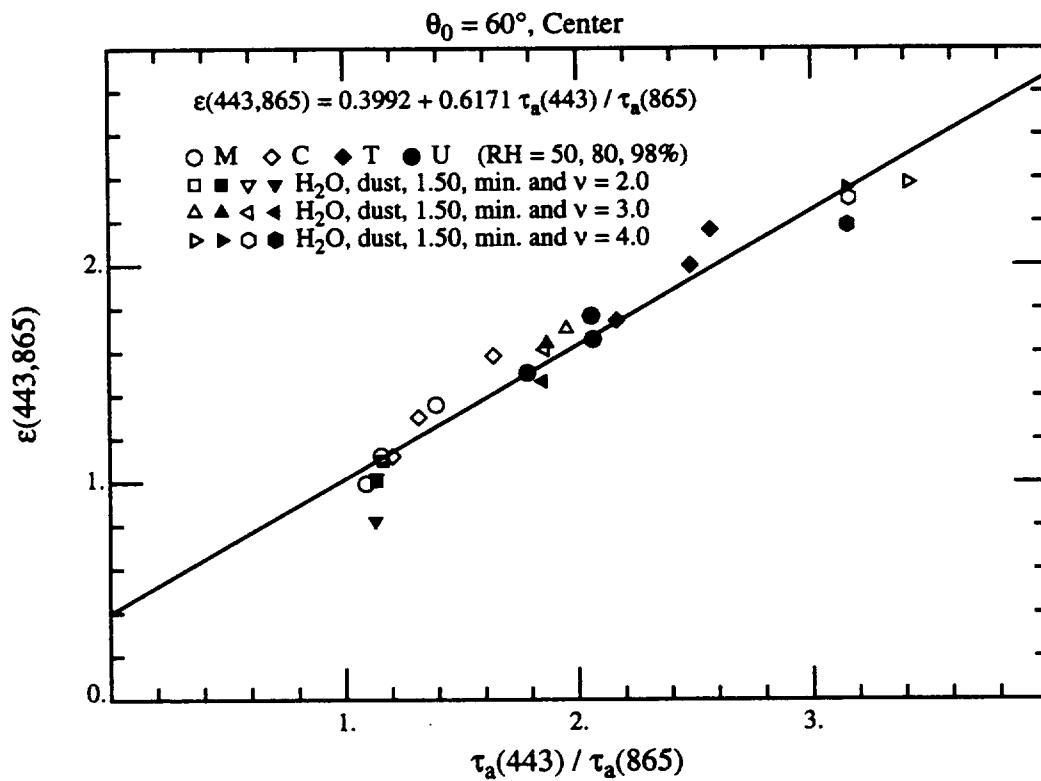


Figure 4. Relationship between  $\tau_a(443)/\tau_a(865)$  and  $\epsilon(443,865)$  at the scan center with  $\theta_0 = 60^\circ$  for several aerosol models. From Gordon [1997].

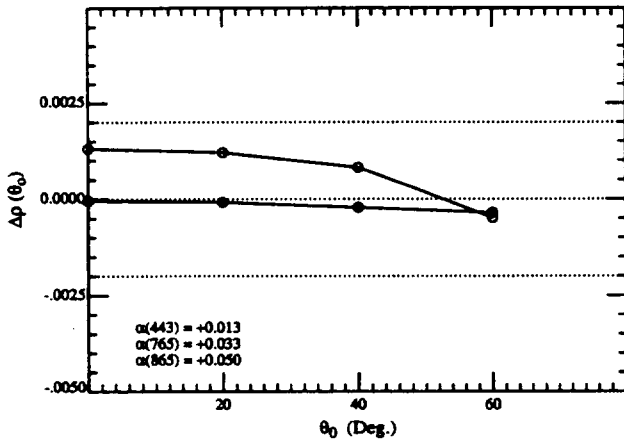


Figure 5a. Error in the retrieved  $t(443)\rho_w(443)$  for viewing near the edge of the scan with a Maritime aerosol at RH = 80% as a function of the solar zenith angle with  $\tau_a(865) = 0.2$  and calibration errors  $\alpha(443)$ ,  $\alpha(765)$ , and  $\alpha(865)$  in Eq. (2) (open circles). Solid circles are for  $\alpha(\lambda_i) = 0$  for all  $\lambda_i$ .

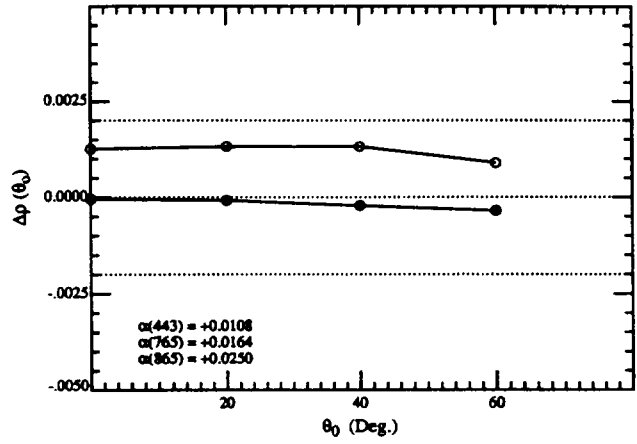


Figure 5b. Error in the retrieved  $t(443)\rho_w(443)$  for viewing near the edge of the scan with a Maritime aerosol at RH = 80% as a function of the solar zenith angle with  $\tau_a(865) = 0.2$  and calibration errors  $\alpha(443)$ ,  $\alpha(765)$ , and  $\alpha(865)$  in Eq. (2) (open circles). Solid circles are for  $\alpha(\lambda_i) = 0$  for all  $\lambda_i$ .

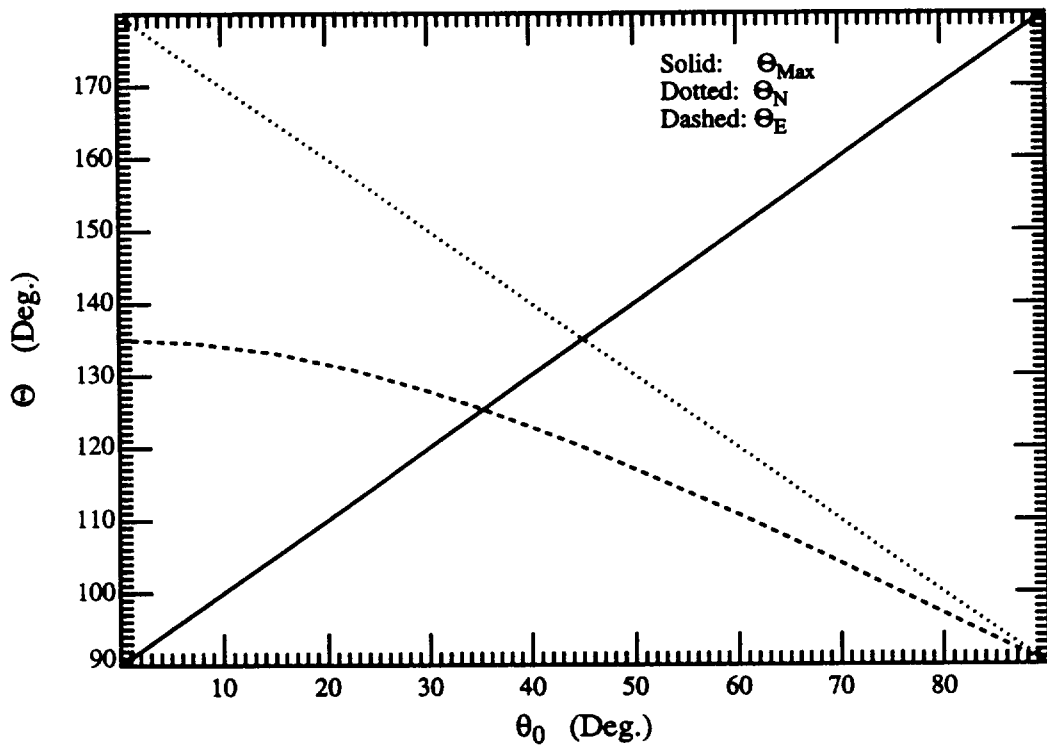


Figure 6.  $\Theta_{Max}$ ,  $\Theta_N$  and  $\Theta_E$  as functions of  $\theta_0$ .

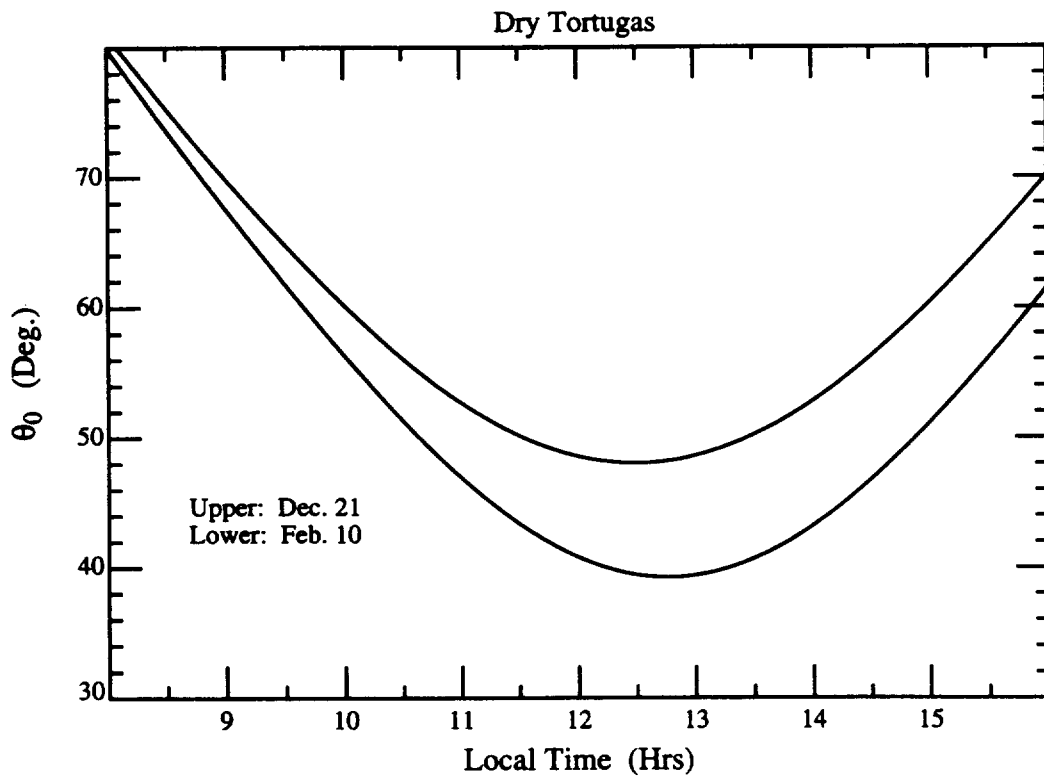


Figure 7.  $\theta_0$  as a function of local time for two days at the Dry Tortugas.